Experimental Eye Research 262 (2026) 110725

Contents lists available at ScienceDirect

Experimental Eye Research

journal homepage: www.elsevier.com/locate/yexer

Research article

Pro-apoptotic shift in human aniridia-derived limbal stromal cells under prolonged high-glucose stress, *In vitro*

Shanhe Liu [a,b,*], Shuailin Li [a,b], Shao-Lun Hsu [a,b], Fabian N. Fries [a,c], Zhen Li [a], Swarnali Kundu [a], Virendra Kumar [a], Berthold Seitz [c], Maryam Amini [a], Shweta Suiwal [a,b], Nóra Szentmáry [a,b], Tanja Stachon [a,b]

[a] Dr. Rolf M. Schwiete Center for Limbal Stem Cell and Congenital Aniridia Research, Saarland University, Homburg, Saar, Germany
[b] Department of Experimental Ophthalmology, Saarland University, Homburg, Saar, Germany
[c] Department of Ophthalmology, Saarland University Medical Center, Homburg, Saar, Germany

ARTICLE INFO

Keywords:
Aniridia
Limbal stromal cells
Apoptosis
High-glucose

ABSTRACT

Metabolic stress can profoundly influence cell survival pathways in limbal stromal cells (LSCs). This study investigated the effects of prolonged supraphysiological glucose exposure on apoptotic responses in both healthy LSCs and LSCs derived from patients with congenital aniridia (AN-LSCs).

Primary human LSCs (n = 12) and AN-LSCs (n = 8) were cultured under high-glucose conditions (70 mM) for either 48 or 72 h. Apoptotic cell populations were quantified using Annexin V/PI flow cytometry. Gene expression of key apoptosis-related markers—*CASP3/7/8/9/10*, *BCL2*, *BAX*, *BID*, *CDKN1A*, *CDKN1B*, *XIAP*, *BIRC5*, and *TNFα*—was assessed by qPCR, and corresponding protein levels were determined via flow cytometry and ELISA.

Both cell types showed a significant increase in apoptosis after 72 h of high-glucose exposure compared to 48 h (LSCs: $p = 0.0021$; AN-LSCs: $p = 0.0017$). At the mRNA level, *CASP3* was upregulated in both cell types ($p = 0.0210$; $p = 0.0396$), while *XIAP* was downregulated ($p = 0.0312$; $p = 0.0141$). In LSCs, *CASP10* and *CDKN1A* (p21) mRNA levels increased ($p = 0.0369$; $p = 0.0495$), whereas *BAX* expression decreased ($p = 0.0097$). In AN-LSCs, *CASP7* level increased ($p = 0.0032$), *BIRC5* (Survivin) expression decreased ($p = 0.0113$). Protein analysis confirmed increased levels of Caspase-3, Caspase-7, and p21 in both groups after 72 h ($p \leq 0.0305$), accompanied by a significant decrease in XIAP ($p = 0.0078$; $p = 0.0348$). Additionally, Survivin protein was markedly reduced in AN-LSCs after prolonged treatment ($p = 0.0182$).

Prolonged high-glucose exposure induces a shift in LSCs from an initial protective state to enhanced apoptotic signaling. This transition, marked by increased pro-apoptotic and reduced anti-apoptotic markers, suggests that sustained metabolic stress can override early survival mechanisms in both LSCs and AN-LSCs. These insights may help guide the development of targeted therapies for aniridia-associated keratopathy.

1. Introduction

Congenital aniridia is a rare, panocular disorder most commonly caused by heterozygous mutations in the PAX6 gene. While classically characterized by iris hypoplasia, the condition encompasses a wide range of ocular abnormalities (Hingorani et al., 2012; Landsend et al., 2021). Among these, aniridia-associated keratopathy (AAK) represents a leading cause of progressive vision loss, affecting the majority of patients over time (Daruich et al., 2023; Latta et al., 2021a; van Velthoven et al., 2023). Traditionally, AAK has been attributed to limbal epithelial stem cell deficiency (LSCD), which results in corneal conjunctivalization, neovascularization, and subsequent visual impairment (Lagali et al., 2013; Landsend et al., 2021; Samant et al., 2016). However, growing evidence highlights the essential role of the underlying limbal stroma in the pathogenesis of AAK (Li et al., 2024, 2025b). The clinical success of techniques like simple limbal epithelial transplantation (SLET), which involves grafting a small piece of donor limbal tissue containing both epithelial and stromal components, underscores the functional importance of the limbal niche in restoring corneal integrity (Borroni et al., 2018). This is further supported by observations of

* Corresponding author. Dr. Rolf M. Schwiete Center for Limbal Stem Cell and Congenital Aniridia Research, Saarland University, Homburg, Saar, Germany.
E-mail address: liushanhe666@gmail.com (S. Liu).

https://doi.org/10.1016/j.exer.2025.110725
Received 26 August 2025; Received in revised form 23 October 2025; Accepted 31 October 2025
Available online 1 November 2025

persistent pathological changes in the limbal stroma itself, such as the loss of marginal corneal arcades following injury, which can be objectively assessed using advanced imaging and correlates with disease outcome (Rocha de Lossada et al., 2020). Dysregulation of extracellular matrix remodeling, impaired epithelial adhesion, and defective wound healing—partially linked to PAX6 haploinsufficiency—further contribute to the complex, multifactorial nature of the disease (Ramaesh et al., 2005).

Limbal stromal cells (LSCs) play a central role in regulating the limbal niche, supporting epithelial stem cell maintenance, facilitating corneal wound healing, and modulating both fibrosis and inflammation (Funderburgh et al., 2016). Importantly, LSCs derived from aniridia patients (AN-LSCs) exhibit intrinsic molecular alterations compared to those from healthy individuals. These changes include reduced *PAX6* expression, dysregulated expression of keratocyte differentiation markers (such as collagens, *ALDH3A1*, and *KER*), and a persistently altered cellular stress response profile (Li et al., 2025c). Strikingly, AN-LSCs display decreased basal levels of NF-κB, a key transcription factor involved in inflammation and cell survival, indicating a fundamentally altered signaling environment within the aniridic limbus (Li et al., 2025a). This intrinsic fragility is further underscored by the heightened sensitivity of AN-LSCs to a range of pharmacological and environmental stressors (Latta et al., 2021b, 2021c; Li et al., 2025a; Pellinen et al., 2012). Taken together, these findings highlight LSCs dysfunction as a major contributor to the pathogenesis of AAK, extending beyond the traditionally emphasized loss of epithelial stem cells.

Metabolic disturbances—particularly hyperglycemia—have profound adverse effects on ocular tissues, including the cornea and limbal region. In individuals with diabetes, complications such as delayed corneal epithelial wound healing and neuropathy are common, largely driven by glucose-induced biochemical imbalances (Brandt et al., 2003). Hyperglycemia disrupts the normal regulation of growth factors, for example by suppressing TGF-β3 while maintaining elevated levels of TGF-β1 (Bettahi et al., 2014), and triggers substantial oxidative and nitrative stress, leading to the accumulation of reactive species that damage cellular structures (Allen et al., 2005). This metabolic stress serves as a potent inducer of apoptosis in various ocular cell types through pathways involving caspase activation and dysregulation of Bcl-2 family proteins, thereby contributing to the spectrum of diabetic complications—from retinal degeneration to corneal endothelial dysfunction (Santos and Kowluru, 2011; Tien et al., 2017; Xu and Yu, 2011). Notably, the early cellular response to metabolic stress may also activate protective mechanisms, such as the transient upregulation of antioxidant defenses (Li et al., 2025b), suggesting that the ultimate impact on cell survival is both context- and time-dependent.

The specific effects of metabolic stress on LSC viability and apoptotic signaling remain insufficiently characterized. Our recent studies demonstrated that exposure to supraphysiological glucose concentrations (70 mM) induces complex, time-dependent alterations in key signaling pathways within primary LSCs (Li et al., 2025b). Short-term exposure (48 h) resulted in the downregulation of pro-fibrotic (TGF-β1) and pro-inflammatory (NF-κB, HIF-1α) mediators—particularly in aniridia-derived LSCs (AN-LSCs)—accompanied by an upregulation of antioxidant gene expression, indicative of an early adaptive response. Interestingly, prolonged glucose exposure (72 h) led to a rebound increase in TGF-β1 and NF-κB expression, notably in healthy LSCs (Li et al., 2025b). Given the dual roles of TGF-β1 and NF-κB in regulating both cell survival and apoptosis, these temporal shifts in signaling suggest that hyperglycemia may critically influence apoptotic pathways in LSCs in a time-dependent manner.

Dysregulated apoptosis is a key determinant of tissue homeostasis and plays a significant role in disease progression. In the context of AAK, inflammatory mediators present in the altered microenvironment—such as TNF-α—may promote apoptosis in residual limbal cells, thereby accelerating LSCD (Li et al., 2025a). In contrast, the activation of effective anti-apoptotic pathways may be essential for preserving the integrity of the limbal niche under stress conditions. The extent to which sustained hyperglycemia influences apoptotic signaling in LSCs, and whether the intrinsic molecular vulnerabilities of AN-LSCs render them more susceptible to such stress, remain critical but unresolved questions. We hypothesized that prolonged high-glucose exposure induces a time-dependent shift toward pro-apoptotic signaling in human LSCs, marked by altered expression of key apoptotic regulators—including caspases, Bcl-2 family proteins, and inhibitor of apoptosis proteins (IAPs)—and that AN-LSCs would demonstrate increased sensitivity to this shift due to their underlying molecular dysregulation.

This study aimed to comprehensively characterize the apoptotic response of primary human LSCs and AN-LSCs to prolonged supraphysiological glucose exposure *in vitro*. Specifically, we evaluated: (1) the kinetics of apoptosis induction at 48 and 72 h using Annexin V/PI flow cytometry; (2) potential differences in apoptotic susceptibility between LSCs and AN-LSCs and (3) the transcriptional and translational regulation of key apoptotic markers, including CASP3/7/8/9/10, BCL2, BAX, BID, CDKN1A (p21), CDKN1B (p27), XIAP, BIRC5 (Survivin), and TNF-α. By integrating these findings with our previous observations on glucose-mediated modulation of TGF-β1 and NF-κB signaling (Li et al., 2025b), this study offers critical insight into how metabolic stress impacts LSCs survival. These results have important implications for understanding the pathogenesis of AAK, particularly in the context of comorbid conditions such as diabetes, which may further destabilize an already compromised limbal niche.

2. Materials and methods

2.1. Ethics statement

All procedures were carried out in accordance with the ethical principles of the Declaration of Helsinki and were approved by the Saarland Ethics Committee, Germany (approval number: 178/22). Written informed consent was obtained from all participants prior to inclusion.

2.2. Human limbal tissue procurement

Limbal biopsies (1.5 mm diameter) were obtained from eight eyes of patients with congenital aniridia undergoing clinically indicated ocular surgeries at the Department of Ophthalmology, Saarland University Medical Center (mean ± SD age: 32.5 ± 17.1 years; range: 2–50 years; 37.5 % male) (Table 1). Before surgery, the severity of AAK was graded using slit-lamp biomicroscope according to the criteria described by Lagali et al. (Ramaesh et al., 2005; Xu and Yu, 2011). Control samples were obtained from twelve healthy donor eyes provided by the LIONS Cornea Bank Saar-Lor-Lux, Trier/Westpfalz (mean age: 73.5 ± 15.5 years; range: 58–89 years; 37.5 % male) (Table 2).

2.3. Primary stromal cell isolation

Human limbal biopsies (1.5 mm in diameter) were enzymatically digested in KGM3 medium (PromoCell, Heidelberg, Germany) supplemented with collagenase A (1 mg/mL; Roche, #10103578001) for 24 h at 37 °C. After enzymatic digestion, mechanical disaggregation was performed following established protocols for LSCs isolation (Li et al., 2025c). The resulting cell suspensions were sequentially filtered through 40 μm Flowmi™ strainers (Bel-Art, #H13680-0040, Wayne, NJ, USA) to remove tissue debris and obtain single-cell suspensions (Li et al., 2025c).

2.4. Cell culture conditions

Cellular aggregates retained on the filter were enzymatically dissociated using 0.05 % trypsin-EDTA (Sigma-Aldrich, Saint Louis, USA) for 5 min, followed by neutralization with DMEM (Thermo Fisher Scientific,

Table 1
Detailed clinical information on the included subjects with congenital aniridia. The table lists the grade of aniridia-associated keratopathy (AAK) based on the classification by Lagali et al. [10, 22], along with each patient's age, gender and the corresponding use of donor material in our measurement series.

Genetic information	AAK Grade	Age (years)	Gender	Experimental methods
PAX6 missense mutation (c.1226-2A > G)	4	43	Male	Quantitative PCR (qPCR)
PAX6 Mutation (c.1191T (q227X))	3	30	Male	qPCR
PAX6 missense Mutation (c.607C > T)	4	12	Male	qPCR/Flow cytometry/ ELISA
PAX6 missense mutation (c.1268A > T)	4	50	Female	qPCR/Flow cytometry/ ELISA
PAX6 missense mutation (c.266A > C)	4	36	Female	qPCR/Flow cytometry/ ELISA
PAX6 deletion (c.753_754delGC)	4	46	Female	qPCR
PAX6 deletion (21q22.12q22. 236,472,360–39,889,694) x1	4	2	Female	qPCR
PAX6 deletion (c.959_960delCA)	3	41	Female	qPCR
Total	3 (25 %); 4 (75 %)	32.50 ± 17.07 (2–50)	5 (62.5 %) Female	

Table 2
Demographic information on the healthy corneal donors included in this study. The table presents donor age and gender, based on data provided by the LIONS Cornea Bank Saar-Lor-Lux, Trier/Westpfalz and the corresponding use of donor material in our measurement series.

Donor number	Age (years)	Gender	Experimental methods
1	89	Male	Quantitative PCR (qPCR)
2	64	Female	qPCR
3	76	Male	qPCR
4	82	Female	qPCR
5	66	Female	qPCR
6	58	Female	qPCR
7	72	Male	qPCR
8	72	Female	qPCR
9	89	Male	Flow cytometry
10	64	Female	Flow cytometry/ELISA
11	76	Male	Flow cytometry/ELISA
12	82	Female	ELISA
Total	74.17 ± 10.06 (58–89)	5 (41.67 %) Male	

Waltham, USA) supplemented with 5 % fetal calf serum (FCS, Thermo Fisher Scientific, Waltham, MA, USA). After centrifugation at 1500×*g* for 5 min, the resulting cell pellets were resuspended in complete DMEM containing 5 % FCS and seeded into 6-well culture plates. Cultures were maintained under standard conditions (37 °C, 5 % CO_2, 95 % humidity), with medium changes every 48–72 h until approximately 90 % confluence was reached.

2.5. Glucose exposure

Based on prior assessments of LSC viability under varying glucose concentrations [8], cells in the present study were cultured for either 48 or 72 h in high-glucose DMEM (70 mM). This supraphysiological glucose concentration was achieved by supplementing standard DMEM with D-glucose (Carl ROTH, Cat. X997, Karlsruhe, Baden-Württemberg, Germany).

2.6. Apoptosis assay

Cellular apoptosis was evaluated using dual staining with Annexin V-APC and propidium iodide (PI) (Invitrogen, #88–8007, Waltham, MA, USA). Trypsinized cell suspensions were washed with binding buffer and incubated with 5 μL Annexin V-APC for 15 min at room temperature, followed by the addition of 5 μL PI. Fluorescence signals were acquired by flow cytometry, with detection channels set to FL4 (660 nm) for Annexin V-APC and FL 2 (585 nm) for PI.

Cells were classified by quadrant analysis as viable (Annexin V^-/PI^-), early apoptotic (Annexin V^+/PI^-), or late apoptotic/necrotic (Annexin V^+/PI^+). Data from three independent experiments were normalized to total cell counts to enable quantitative comparison across experimental conditions. Cells from 3 healthy LSC donors and 3 AN-LSC donors were used for this analysis. Sample selection is shown in Tables 1 and 2 For each donor, the assay was performed in technical triplicate.

2.7. RNA extraction and cDNA synthesis

Total RNA was extracted using the NORGEN RNA Purification Plus Micro Kit according to the manufacturer's instructions (Norgen Biotek, Ontario, Canada). RNA purity was assessed spectrophotometrically (Analytik Jena AG, Jena, Germany), with A260/A280 ratios consistently exceeding 1.8. For cDNA synthesis, 500 ng of total RNA was reverse-transcribed using the OneTaq RT-PCR Kit (New England Biolabs Inc., Ipswich, USA). All RNA and cDNA samples were stored at −80 °C and −20 °C until further use.

2.8. qPCR

Gene expression analysis was performed using SYBR Green-based quantitative PCR (qPCR) assays (Vazyme, Nanjing, China). Primer sequences used in the study are listed in Table 3. Each 10 μL reaction contained 1 μL cDNA, 1 μL Qiagen primer mix, 5 μL SYBR Green Master Mix, and 3 μL nuclease-free water. Amplification was carried out on a QuantStudio 5 Real-Time PCR System (ThermoFisher Scientific™ GmbH, Dreieich, Germany) under the following cycling conditions: initial denaturation at 95 °C for 10 s, annealing at 60 °C for 30 s, and extension at 72 °C for 15 s, for a total of 40 cycles. Relative gene expression was quantified using the 2^−ΔΔCt method, with *β*-glucuronidase (*GUSB*) used as the endogenous reference gene. The analysis was conducted using cells from 8 donors per group (LSCs and AN-LSCs). Sample selection is shown in Tables 1 and 2 Each qPCR reaction was run in duplicate.

Table 3
Specifications of the primers used for SYBR Green-based real-time PCR analysis.

Target Transcript	Catalog Reference	Fragment Size (bp)	Transcript ID (NCBI)
BAX	QT00031192	111	NM_004324
BCL2	QT00025011	80	NM_000633
BID	QT00077833	98	NM_001196
CASP3	QT00023947	147	NM_004346
CASP7	QT00003549	149	NM_001227
CASP8	QT00052416	61	NM_001080124
CASP9	QT00036267	102	NM_001229
CASP10	QT00002394	91	NM_001206542
CDKN1A	QT00062090	79	NM_000389
CDKN1B	QT00998445	146	NM_004064
GUSB	QT00046046	96	NM_000181
BIRC5	QT00081186	101	NM_001168
TNF	QT00029162	98	NM_000594
XIAP	QT00042854	87	NM_001167

2.9. Flow cytometry

Marker expression was analyzed following cell dissociation with non-EDTA trypsin (Invitrogen, SM-2003, Waltham, MA, USA). Cells were incubated with the primary antibodies listed in Table 4 and subsequently stained with fluorescein isothiocyanate (FITC)-conjugated secondary antibodies (Antibody Online, No. ABIN101988, Aachen, Germany; Bio-Techne, No. F0118, Wiesbaden, Germany). For internal negative controls, the primary antibody was omitted while all other procedures remained identical. During flow cytometry, the primary cell population was gated using FSC-A and SSC-A parameters to exclude debris, and single cells were identified by FSC-A versus FSC-H plotting to eliminate aggregates. Protein expression was quantified as mean fluorescence intensity (MFI) from histograms generated with CytExpert software (Beckman Coulter GmbH, Krefeld, Germany). Protein level analysis was performed on cells from 3 donors per group. Sample selection is shown in Tables 1 and 2 The measurements for each donor were conducted in technical duplicate.

2.10. Enzyme-linked immunosorbent assay (ELISA)

ELISA assay was performed from cell culture supernatants obtained after 48h or 72h exposure with 70 nM glucose concentration. Secreted TNF-α levels were measured using the DuoSet ELISA kit (R&D Systems, #DY210, Minneapolis, MN, USA) according to the manufacturer's instructions. Absorbance was recorded at 450 nm using a Tecan F50 microplate reader (TECAN Deutschland GmbH, Crailsheim, Germany). Cytokine concentrations were normalized to total protein content, as determined by the bicinchoninic acid (BCA) assay. Cells from 3 healthy LSC donors and 3 AN-LSC donors were used for this analysis. Sample selection is shown in Tables 1 and 2 The measurements for each donor were conducted in technical duplicate.

Table 4
List of antibodies and detection reagents used for flow cytometry analysis.

Marker Target	Clone/Type	Reactivity	Working Dilution	Vendor
BAX	E4U1V mAb (rabbit)	Human	1:100	Cell Signaling, Danvers, MA, USA
BCL-2	Polyclonal (rabbit)	Human	1:100	Proteintech, Wuhan, China
BID	Polyclonal (rabbit)	Human	1:100	Proteintech, Wuhan, China
Caspase-3	Polyclonal (rabbit)	Human	1:100	Proteintech, Wuhan, China
Caspase-9	Polyclonal (rabbit)	Human	1:100	Cell Signaling, Danvers, MA, USA
Caspase-10	Polyclonal (rabbit)	Human	1:100	Proteintech, Wuhan, China
Cleaved Caspase-7	D6H1 mAb (rabbit)	Human	1:100	Cell Signaling, Danvers, MA, USA
Cleaved Caspase-8	E6H8S mAb (rabbit)	Human	1:100	Cell Signaling, Danvers, MA, USA
Goat anti-Rabbit IgG (Heavy & Light Chain) Antibody (FITC)	Preadsorbed	Secondary	1:500	Antibody Online, Aachen, Germany
Goat anti-Mouse IgG (FITC)	REAfinity	Secondary	1:50	Miltenyi Biotec, Wiesbaden, Germany
p21 (CDKN1A)	12D1 mAb (rabbit)	Human	1:100	Cell Signaling, Danvers, MA, USA
p27 (CDKN1B)	SX53G8.5 mAb (mouse)	Human	1:100	Cell Signaling, Danvers, MA, USA
Survivin	71G4B7 mAb (rabbit)	Human	1:100	Cell Signaling, Danvers, MA, USA
TNF-α	D1G2 mAb (rabbit)	Human	1:100	Cell Signaling, Danvers, MA, USA
XIAP	Polyclonal (rabbit)	Human	1:100	Proteintech, Wuhan, China

2.11. Statistical analysis

Data normality was assessed using the Shapiro–Wilk test. Concentration-dependent effects were analyzed by two-way ANOVA followed by Dunnett's post hoc test, using GraphPad Prism 9.0. qPCR results are presented as geometric mean ± standard deviation (SD), while flow cytometry and ELISA data are expressed as arithmetic mean ± SD. A p-value of <0.05 was considered statistically significant.

3. Results

3.1. Apoptotic cell ratio

Flow cytometry analysis demonstrated a significant increase in apoptosis in both LSCs ($p = 0.0021$) and AN-LSCs ($p = 0.0017$) after 72 h of exposure to 70 mM glucose. At this time point, apoptosis rates were elevated approximately threefold in LSCs and fourfold in AN-LSCs compared to the 48-h exposure. Nevertheless, no significant differences in apoptosis rates were observed between LSCs and AN-LSCs at either 48 or 72 h of high-glucose exposure ($p \geq 0.0958$) (Fig. 1).

3.2. mRNA levels of apoptosis-related markers

After 72 h of high-glucose exposure, *CASP3* mRNA levels were significantly upregulated in both LSCs and AN-LSCs ($p = 0.0210$; $p = 0.0396$), while *XIAP* expression was significantly downregulated ($p = 0.0312$; $p = 0.0141$). In LSCs, *CASP10* and *CDKN1A* (p21) mRNA levels were also significantly elevated at 72 h compared to 48 h ($p = 0.0369$; $p = 0.0495$), whereas *BAX* expression was significantly decreased ($p = 0.0097$). In AN-LSCs, high-glucose exposure led to a significant increase in *CASP7* mRNA levels ($p = 0.0032$) and a significant decrease in *BIRC5 (Survivin)* expression ($p = 0.0113$) at 72 h relative to 48 h. None of the other analyzed mRNAs showed significant differences by qPCR ($p \geq 0.0801$) (Fig. 2).

3.3. Protein levels of apoptosis-related markers

Protein levels of Caspase-3 and Caspase-7 were significantly upregulated in both LSCs and AN-LSCs after 72 h of 70 mM glucose treatment ($p \leq 0.0305$; $p \leq 0.0108$). In contrast, protein levels of Bcl-2 family members showed no significant changes in any of the groups analyzed ($p \geq 0.6465$). Notably, p21 protein expression was significantly increased in both cell types at 72 h ($p = 0.0157$; $p = 0.0220$), while XIAP protein levels were significantly reduced ($p = 0.0078$; $p = 0.0348$). Furthermore, Survivin protein level was significantly decreased in AN-LSCs after 72 h compared to 48 h of high-glucose conditioning ($p = 0.0182$). By contrast, TNFα protein levels remained unchanged, as assessed by both flow cytometry and ELISA ($p \geq 0.3115$) (Figs. 3–5).

4. Discussion

As previously reported, the apoptosis rate of AN-LSCs under normoglycemic conditions is significantly higher than that of healthy LSCs (Liu et al., 2025a). In contrast, in the present study, no significant difference in apoptotic rates was observed between LSCs and AN-LSCs after 48 or 72 h of high-glucose exposure. Both cell types exhibited a measurable response to hyperglycemic stress.

A prior investigation focused specifically on the effects of 48 h of

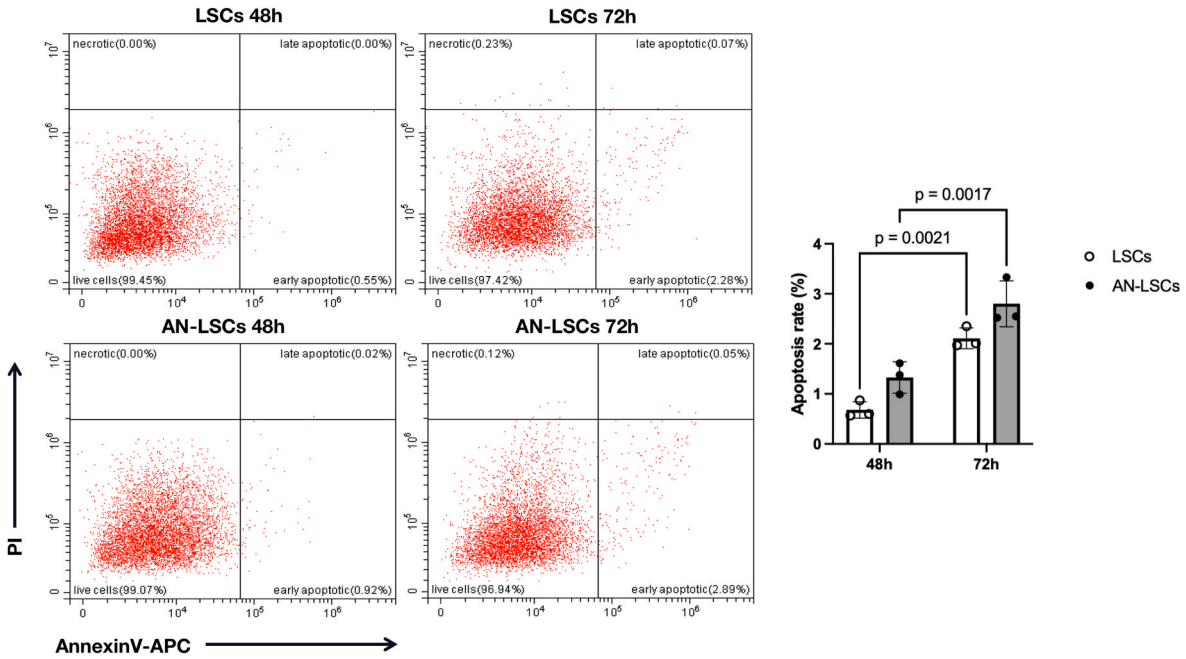

Fig. 1. Apoptotic rates of limbal stromal cells (LSCs) and aniridia-LSCs (AN-LSCs), following exposure to 70 mM glucose for 48 or 72 h (n = 3).
LSCs and AN-LSCs were cultured in medium containing 70 mM glucose for either 48 or 72 h, stained with Annexin V-APC and propidium iodide (PI), and analyzed by flow cytometry. Data are presented as mean ± SD from three independent experiments. Statistical significance was determined using two-way ANOVA followed by Dunnett's post hoc test; significant p-values are indicated. Apoptosis was significantly increased in both LSCs ($p = 0.0021$) and AN-LSCs ($p = 0.0017$) after 72 h of exposure compared to 48 h.

exposure to high glucose (70 mM) (Liu et al., 2025b). At this early time point, both healthy LSCs and aniridia-derived AN-LSCs displayed a pronounced anti-apoptotic shift, characterized by downregulation of pro-apoptotic markers and concomitant upregulation of survival-associated factors. Notably, the anti-apoptotic proteins XIAP and Survivin were elevated at both mRNA and protein levels, indicating suppression of caspase-mediated apoptotic pathways. These protective responses were particularly marked in AN-LSCs, which showed a greater reduction in apoptosis and a relatively higher induction of anti-apoptotic markers during the 48-h high-glucose challenge (Liu et al., 2025b). Collectively, these findings suggested that LSCs—especially those derived from aniridia patients—are capable of activating an intrinsic survival program in response to acute metabolic stress.

Despite the initial protective phase, the present study has shown that prolonged high-glucose exposure led to a reversal of these trends. Extending the treatment duration from 48 to 72 h resulted in a significant increase in apoptosis in both LSCs and AN-LSCs, indicating that the early adaptive response was ultimately unsustainable. By 72 h, the protein levels of the executioner caspases—Caspase-3 and Caspase-7—were markedly elevated, reflecting activation of the terminal apoptotic cascade. Concurrently, anti-apoptotic defenses began to decline. XIAP levels were significantly reduced in both cell types, and in AN-LSCs, Survivin (*BIRC5*) expression dropped sharply at 72 h compared to the 48-h time point. The loss of these critical inhibitors likely removed an essential block on caspase activity, thereby facilitating apoptosis. In addition, a significant upregulation of p21 was observed both in healthy LSCs and AN-LSCs by 72 h (Fig. 6). This suggests a p21-mediated cell cycle arrest mechanism, which may act as a temporary protective response by halting proliferation and allowing DNA damage repair (Currier et al., 2019; Shamloo and Usluer, 2019). However, despite these efforts, the overall apoptotic ratio increased, underscoring the insufficiency of endogenous defense mechanisms in counteracting sustained metabolic stress, in both cell types (Fig. 6).

The contrasting cellular responses observed between 48 and 72 h highlight the dynamic and time-dependent nature of the stress response to hyperglycemia. In the early phase, high glucose appears to activate signaling pathways that favor cell survival (Liu et al., 2025b). Indeed, acute hyperglycemia has been shown to induce transient adaptive mechanisms in various cell types. For example, short-term high-glucose exposure in cardiac fibroblasts has been reported to enhance proliferative and anti-apoptotic signaling (Zhang et al., 2021), which aligns with our observations in LSCs. We propose that during the initial 24–48 h of hyperglycemic stress, LSCs mount a protective response characterized by enhanced antioxidant defenses and suppression of inflammatory signaling, enabling them to buffer against the sudden metabolic surplus. This is consistent with our previous findings, where acute high-glucose treatment downregulated pro-inflammatory mediators such as NF-κB and TGF-β1, while upregulating antioxidant genes in limbal fibroblasts—thereby creating a cellular environment less conducive to apoptosis (Li et al., 2025b). Over prolonged exposure, however, the protective balance shifts, as sustained hyperglycemia imposes cumulative cellular damage. Chronic high-glucose conditions are well documented to promote the generation of reactive oxygen species (ROS) and advanced glycation end-products (AGEs), which activate stress kinases such as JNK and p38, along with pro-inflammatory signaling cascades (Cepas et al., 2020; Chen et al., 2018; Dobi et al., 2019; Shi et al., 2013). These effects initiate a self-perpetuating cycle of oxidative stress, inflammation, and apoptosis—a hallmark of diabetic tissue pathology (Kim et al., 2011; Taguchi and Fukami, 2023). Consistent with this notion, our previous work showed that after 48 h of 70 mM glucose exposure, LSCs exhibited significantly reduced TGF-β1, NFκB, and HIF-1α expression, alongside marked upregulation of the antioxidant regulators Nrf2 and catalase, indicating an early anti-fibrotic, anti-inflammatory, and antioxidant phenotype. By contrast, at 72 h 70 mM glucose exposure, TGF-β1 and NFκB expression increased while Nrf2 and catalase were suppressed, reflecting a shift toward a pro-fibrotic and pro-inflammatory profile. Such pathway reactivation, in conjunction with oxidative and inflammatory stress, may undermine the initial anti-apoptotic state and contribute to the pro-apoptotic shift observed in the present study (Li et al., 2025a). In this subject, LSCs appeared to transition into this detrimental phase by 72 h. The resurgence of

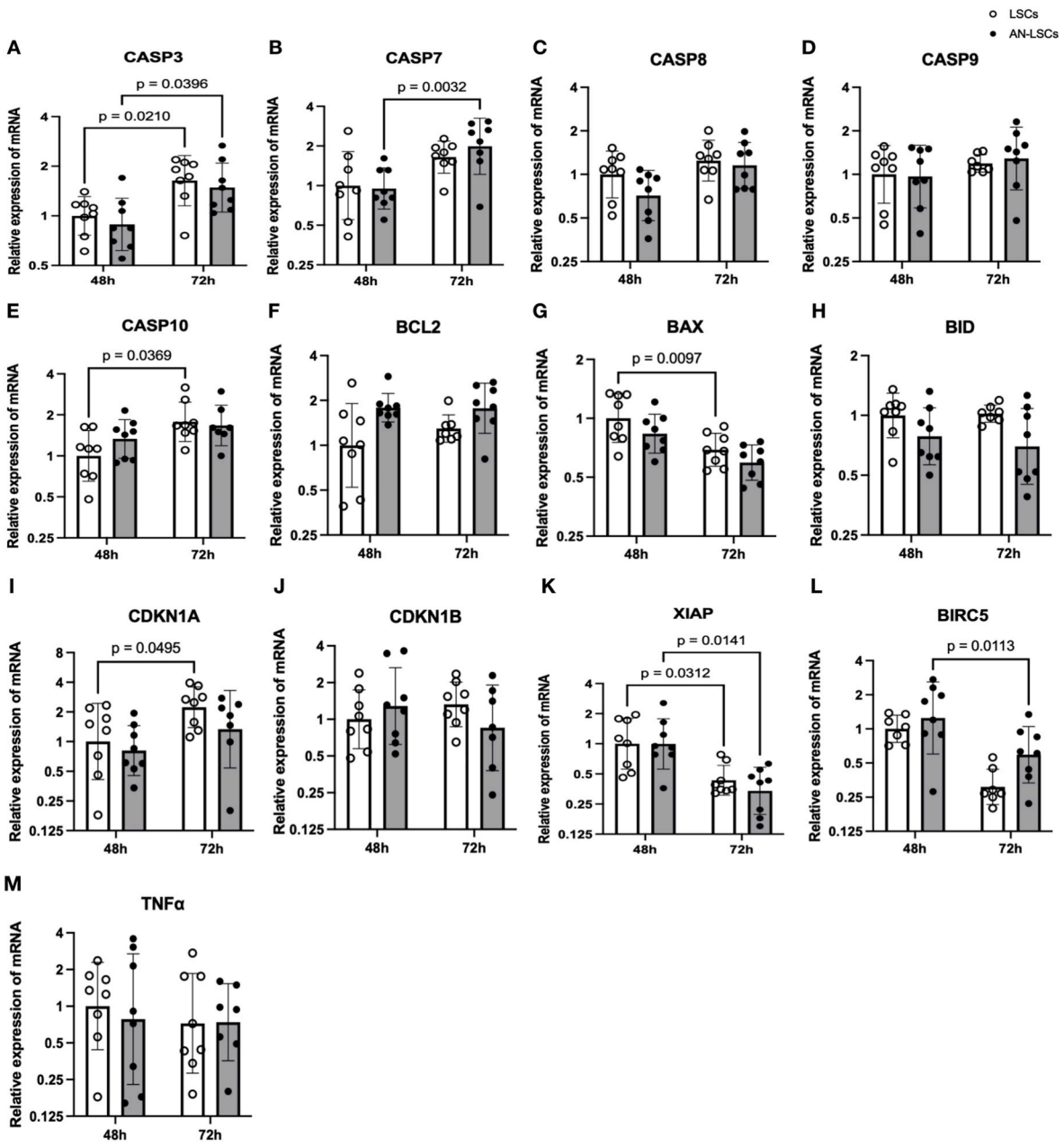

Fig. 2. mRNA levels of CASP family markers (A–E), BCL2 family markers (F–H) and other apoptosis-related markers (I–M) in limbal stromal cells (LSCs) and aniridia-LSCs (AN-LSCs), following exposure to 70 mM glucose for 48 or 72 h (n = 8).
CASP3, CASP7, CASP8, CASP9 and *CASP10* mRNA levels (A-E), *BCL2, BAX* and *BID* mRNA levels (F-H) and *CDKN1A, CDKN1B, TNFα, XIAP* and *BIRC5* mRNA levels (I-M) are shown. Values are presented on a logarithmic (log_2) scale as geometric mean ± geometric standard deviation. Statistical significance was assessed using two-way ANOVA followed by Dunnett's post hoc test; significant p-values are indicated. *CASP3* mRNA was significantly upregulated in both LSCs and AN-LSCs at 72 h (p = 0.0210; p = 0.0396), while *XIAP* was significantly downregulated in both cell types (p = 0.0312; p = 0.0141). In LSCs, *CASP10* and *CDKN1A* were significantly upregulated at 72 h (p = 0.0369; p = 0.0495), whereas *BAX* was significantly downregulated (p = 0.0097). In AN-LSCs, *CASP7* was significantly upregulated (p = 0.0032) and *BIRC5* (*Survivin*) expression was significantly reduced at 72 h compared to 48 h (p = 0.0113).

apoptosis at this time point likely reflects an accumulation of oxidative and inflammatory stress signals, even though these were not directly measured. Notably, in healthy LSCs, we observed significant upregulation of *CASP10* at 72 h, suggesting renewed activation of extrinsic apoptotic pathways. The same phenomenon could be observed in AN-LSCs, regarding *CASP7*. It is plausible that prolonged high-glucose exposure induces the release of death ligands or pro-inflammatory cytokines within the culture environment, re-engaging NF-κB and triggering Caspase-8/10 activation (Liu et al., 2025a). Once these initiator caspases are active, they drive cleavage of Caspase-3 and -7, thereby overriding the anti-apoptotic protections observed during the earlier adaptive phase. Simultaneously, anti-apoptotic defenses began to collapse. XIAP and Survivin levels declined significantly at 72 h—particularly in AN-LSCs, where the loss of Survivin was most pronounced. Given that Survivin is essential for both cell cycle progression and inhibition of apoptosis, its reduction in AN-LSCs suggests that these cells lose their adaptive survival advantage more rapidly under prolonged metabolic stress, than LSCs. This may be partly attributable to the inherently lower baseline expression of key survival proteins in AN-LSCs. Previous studies have shown that AN-LSCs exhibit reduced basal levels of Bcl-2, XIAP, and Survivin, predisposing them to apoptosis even under normal conditions (Liu et al., 2025a). Indeed, AN-LSCs

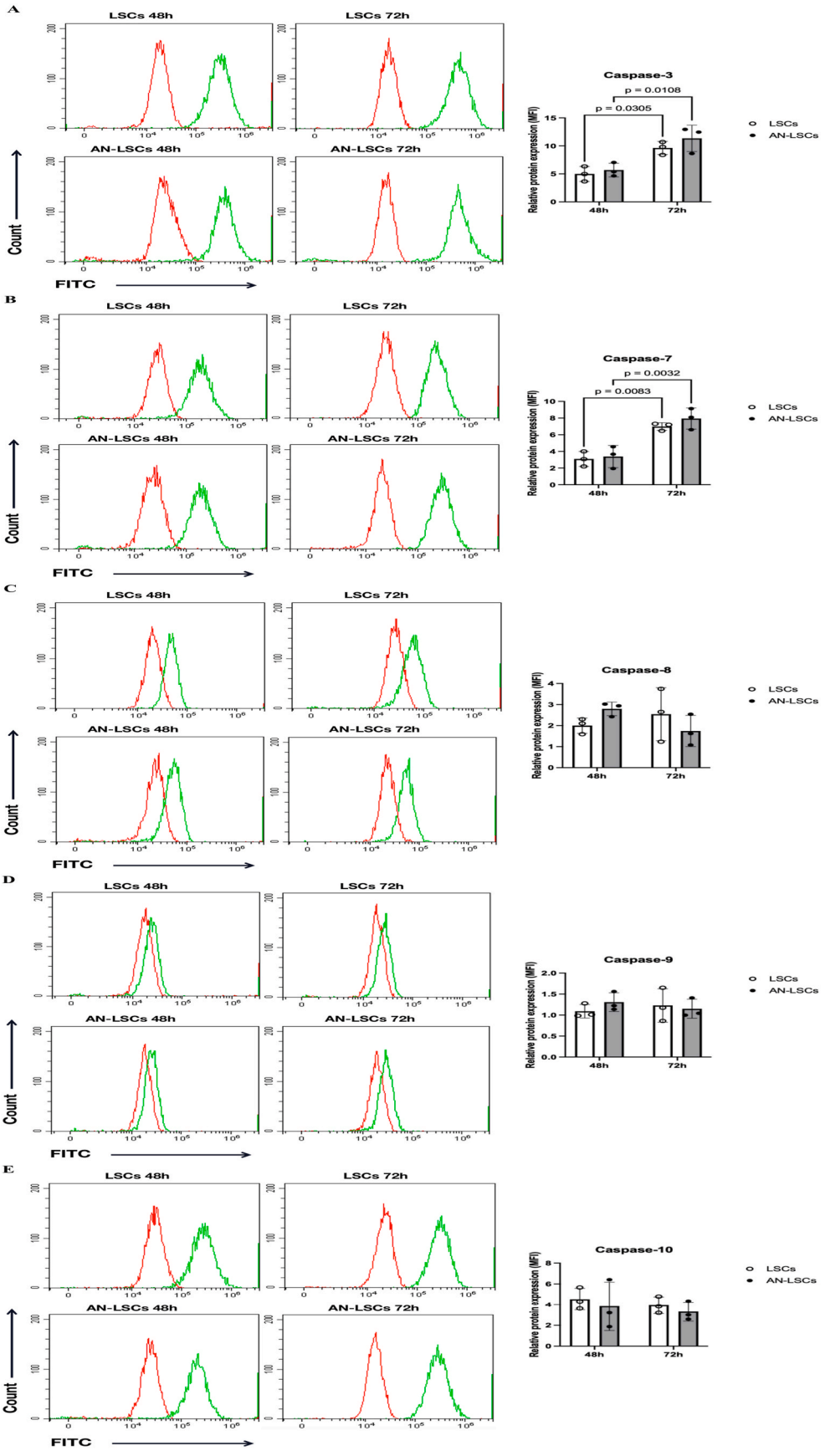

(caption on next page)

Fig. 3. Protein levels of Caspase family markers in limbal stromal cells (LSCs) and aniridia-LSCs (AN-LSCs), following exposure to 70 mM glucose for 48 or 72 h, using flow cytometry (A–E) (n = 3).
Protein levels of Caspase-3, Caspase-7, Caspase-8, Caspase-9, and Caspase-10 were assessed. Data represent mean ± standard deviation (SD) from three independent experiments. Statistical significance was determined using two-way ANOVA followed by Dunnett's post hoc test; significant p-values are indicated. Representative flow cytometry histograms show primary antibody staining (green) and the corresponding secondary antibody-only control (red). Mean fluorescence intensity (MFI) values are normalized to secondary antibody controls. Protein level of Caspase-3 and Caspase-7 was significantly upregulated in both LSCs and AN-LSCs at 72 h compared to 48 h ($p \leq 0.0305$; $p \leq 0.0108$).

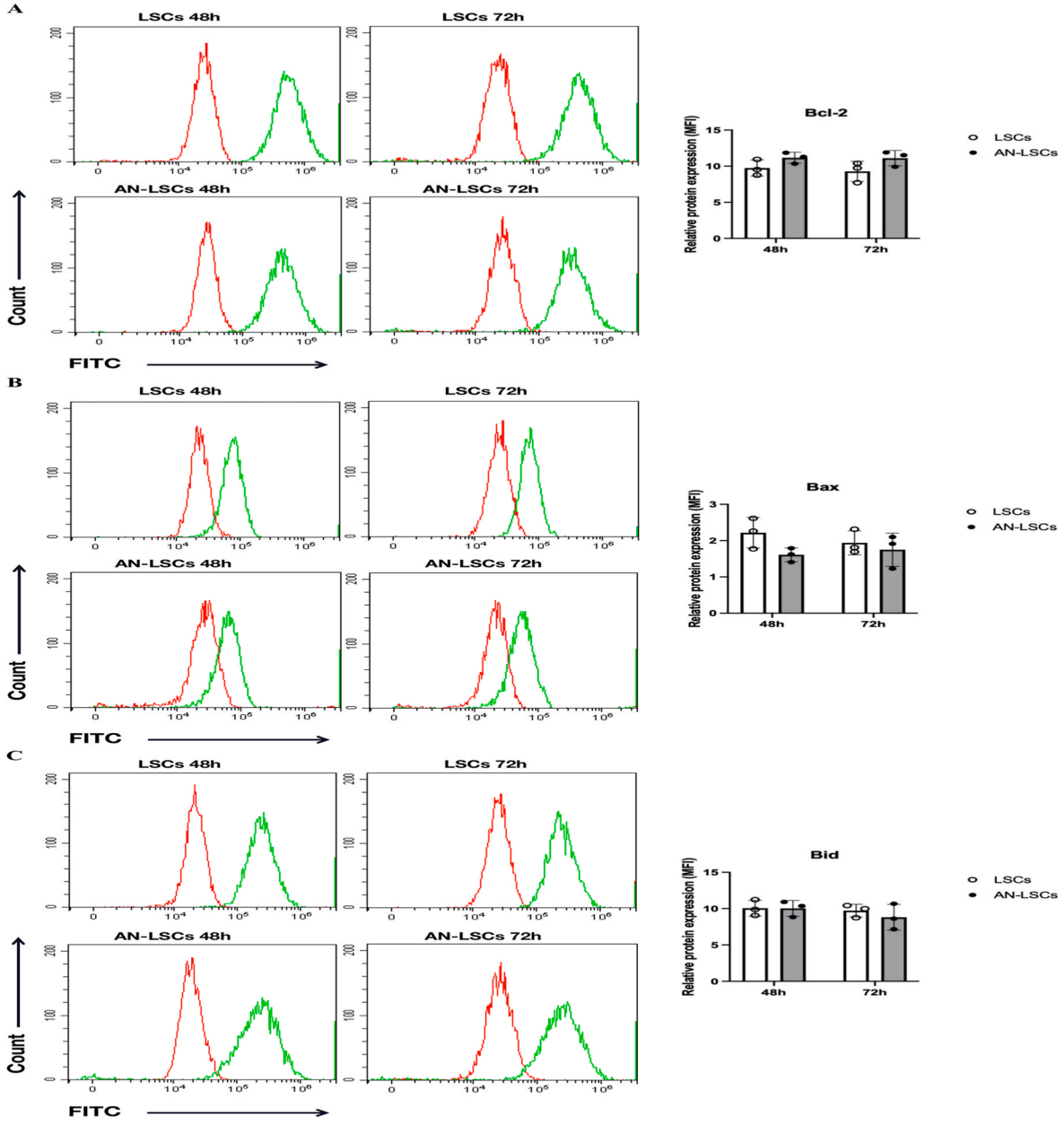

Fig. 4. Protein levels of Bcl-2 family markers in limbal stromal cells (LSCs) and aniridia-LSCs (AN-LSCs), following exposure to 70 mM glucose for 48 or 72 h, using flow cytometry (A–C) (n = 3).
Protein levels of Bcl-2, Bax, and Bid were analyzed. Data are presented as mean ± standard deviation (SD) from three independent experiments. Statistical analysis was performed using two-way ANOVA followed by Dunnett's post hoc test; significant p-values are indicated. Representative histograms show primary antibody staining in green and the corresponding secondary antibody-only control in red. Mean fluorescence intensity (MFI) values are normalized to secondary antibody controls. No significant differences in the protein expression levels of Bcl-2, Bax, or Bid were observed in any of the analyzed subgroups ($p \geq 0.6465$).

typically demonstrate higher baseline apoptosis rates than their healthy counterparts (Liu et al., 2025a).

In summary, while both healthy and AN-LSCs exhibit an early, short-lived resistance to glucose-induced apoptosis, AN-LSCs appear to exhaust their defenses more rapidly. This accelerated vulnerability may contribute to disease progression in AAK, particularly under conditions of metabolic stress such as diabetes. These results extend our understanding of how metabolic stress may contribute to ocular surface disease. Transient hyperglycemia appears to induce an adaptive survival response in LSCs, potentially serving as a protective mechanism to

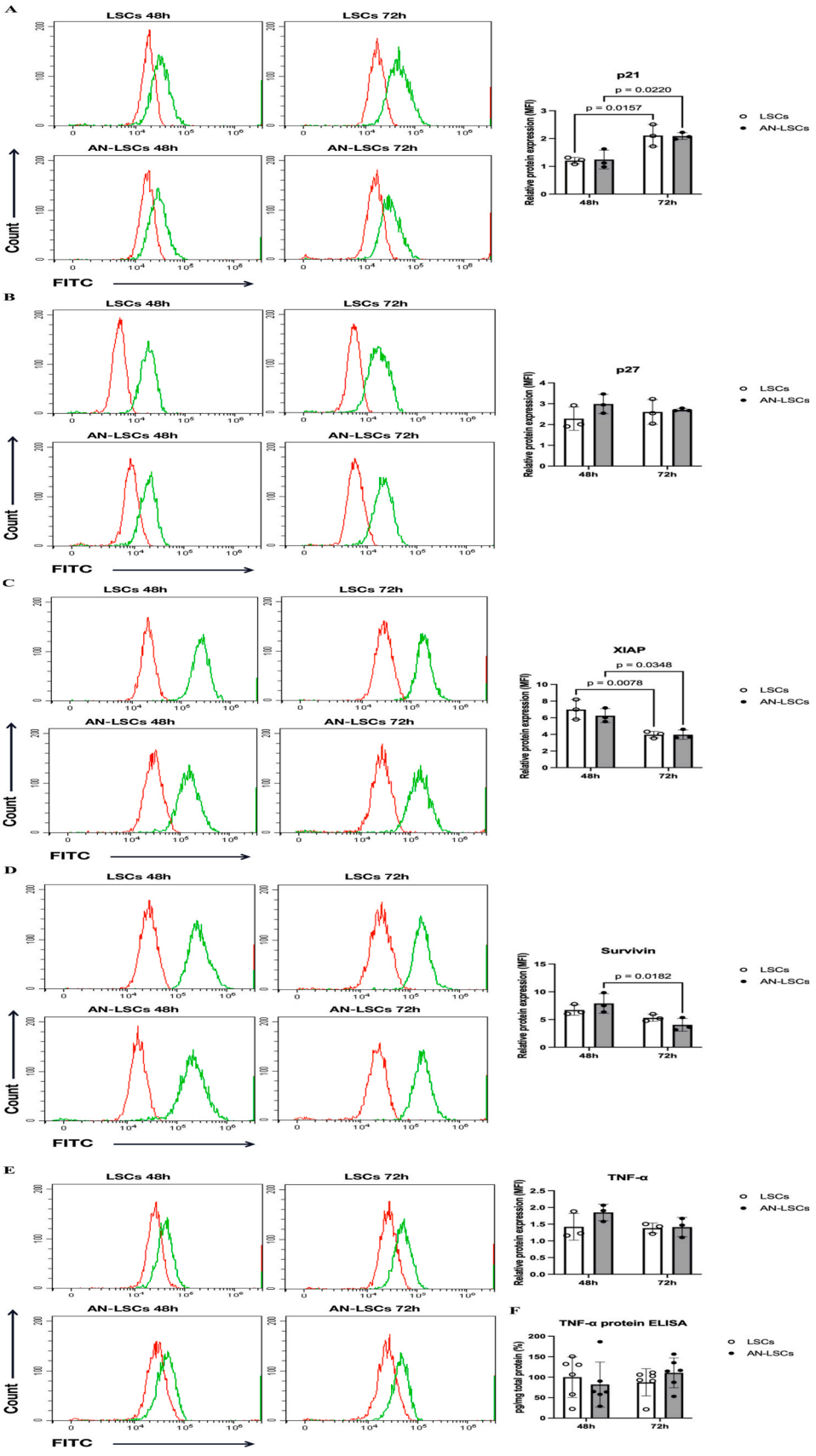

(caption on next page)

Fig. 5. Protein levels of other apoptosis-related markers in limbal stromal cells (LSCs) and aniridia-LSCs (AN-LSCs), following exposure to 70 mM glucose for 48 or 72 h, using flow cytometry (A–E) and ELISA (F) (n = 3).
Protein levels of p21, p27, XIAP, TNF-α, and Survivin are shown. Data are presented as mean ± standard deviation (SD) from three independent experiments. Statistical analysis was performed using two-way ANOVA followed by Dunnett's post hoc test; significant p-values are indicated. Representative histograms show primary antibody staining in green and the corresponding secondary antibody-only control in red. Mean fluorescence intensity (MFI) values are normalized to secondary antibody controls. p21 protein levels were significantly upregulated ($p = 0.0157$; $p = 0.0220$) and XIAP protein levels were significantly downregulated ($p = 0.0078$; $p = 0.0348$) in both LSCs and AN-LSCs from 48 to 72 h. In AN-LSCs, Survivin protein levels were significantly lower at 72 h compared to 48 h ($p = 0.0182$). No significant changes were observed in the protein levels of p27 or TNF-α from 48 to 72 h ($p \geq 0.3115$).

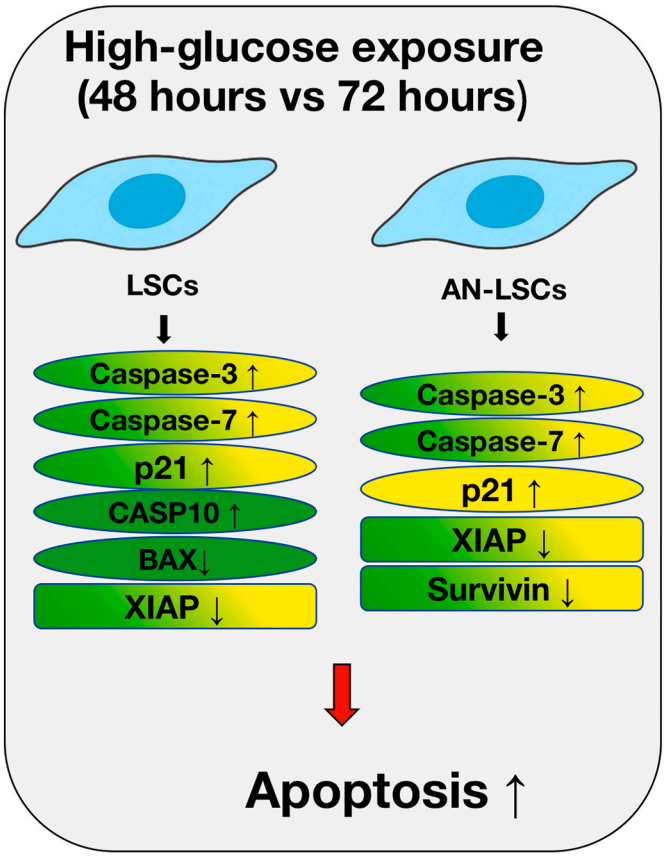

Fig. 6. Molecular changes in limbal stromal cells (LSCs) and aniridia-derived LSCs (AN-LSCs) following exposure to 70 mM glucose for 48 vs 72 h.
A schematic illustration depicts key apoptotic signaling changes in LSCs and AN-LSCs comparing 48 h of high-glucose exposure to 72 h. Color coding represents the level of regulation: green indicates changes at the mRNA level, yellow at the protein level, and green-yellow at both mRNA and protein levels. Oval markers indicate pro-apoptotic molecules, and square markers indicate anti-apoptotic molecules. The upregulation of pro-apoptotic markers Caspase-3, Caspase-7, and p21 was observed alongside a downregulation of the anti-apoptotic proteins XIAP and Survivin, indicating a time-dependent shift toward apoptosis in both LSCs and AN-LSCs. An additional upregulation of the pro-apoptotic Caspase-10, accompanied by a downregulation of the pro-apoptotic Bax, was observed exclusively in LSCs, whereas this trend was not observed in AN-LSCs. Furthermore, a downregulation of the pro-apoptotic Survivin, was observed only in AN-LSCs, whereas this trend was not observed in LSCs.

preserve the limbal stem cell niche during short-term metabolic fluctuations. However, with sustained hyperglycemia, this protective effect is lost, and apoptotic pathways become strongly activated. This shift may lead to depletion of stromal support cells and, in turn, exacerbate limbal stem cell deficiency. In the context of diabetes or AAK, our findings suggest that chronic hyperglycemia could accelerate damage to the corneal limbus by promoting stromal cell apoptosis after an initial period of cellular quiescence. These observations are consistent with previous studies reporting delayed corneal wound healing and increased cell loss in diabetic patients, typically observed only under conditions of persistent hyperglycemia (Buonfiglio et al., 2024). The pronounced early anti-apoptotic response seen in AN-LSCs suggests a potential therapeutic window during which cytoprotective interventions could be most effective. Enhancing antioxidant and anti-apoptotic mechanisms—for example, through caspase inhibitors or agents that stabilize XIAP and Survivin—might prolong stromal cell survival during the early phase of metabolic stress (Kim and Li, 2013; Souers et al., 2013). Conversely, targeting late-stage stress mediators—such as with ROS scavengers or TNF-α inhibitors—could help prevent the subsequent rise in apoptosis (Foster et al., 2003). Future studies should explore such therapeutic strategies and determine whether a similar biphasic response occurs *in vivo*.

It is important to acknowledge the limitations inherent to this *in vitro* study. One key consideration is the age difference between the aniridia patient cohort and the control cadaveric donors. Our primary objective was to investigate the intrinsic differences between limbal stromal cells derived from healthy and aniridic eyes. All cell cultures were maintained under identical conditions and used at low passages to minimize the potential impact of senescence-related changes. Nevertheless, the possible influence of age-associated factors cannot be completely excluded.

Furthermore, subclinical or undiagnosed metabolic conditions in older donors—such as diabetes, which is known to alter corneal cell function and wound healing—could represent an additional source of variability. Thus, the advanced age of the control donors may have introduced unrecognized confounding variables. It should be noted, however, that all control samples were obtained from cadaveric donors classified as healthy, with no recorded ocular pathology or history of diabetes, thereby reducing the likelihood of significant systemic confounders.

While the principal apoptotic patterns identified in this study were consistent across donors, it should be acknowledged that the sample size—although considerable given the rarity of the disease—may not have been sufficient to detect more nuanced, donor-specific variations. Future investigations involving larger and more diverse cohorts will be essential to validate the generalizability of these findings and to delineate potential subpopulations with distinct sensitivities to metabolic stress.

Other limitations include the use of a supraphysiological glucose concentration (70 mM) and a defined culture system, which cannot fully replicate the complex *in vivo* limbal microenvironment involving interactions with immune cells, nerves, and vasculature. Furthermore, the 72-h observation period captured a specific biphasic response but not long-term cellular outcomes. Although key alterations in apoptotic markers were identified, the upstream signaling drivers, such as specific kinase pathways and reactive oxygen species, warrant further investigation. Finally, while the sample size is substantial for a rare disease, some donor-to-donor variability may exist.

Notwithstanding these limitations, our findings offer insightful clinical implications. The identified biphasic response, an initial protective state followed by apoptotic collapse, provides a potential mechanism underlying the progressive nature of AAK. The pronounced early anti-apoptotic response, particularly in AN-LSCs, reveals a critical "therapeutic window." During this period, interventions aimed at enhancing endogenous survival pathways, such as topical caspase inhibitors, XIAP/Survivin stabilizers, or antioxidants, could be

strategically applied to prolong stromal cell viability. Conversely, in advanced disease with chronic stromal cell loss, our results support the exploration of cell-based therapies, including transplantation of healthy LSCs, to regenerate a functional limbal niche. Thus, this work outlines a direction for developing targeted therapies to preserve vision in patients with AAK.

5. Conclusions

This study demonstrates that prolonged glucose exposure (72 h) led to a marked increase in apoptosis, characterized by upregulation of caspases and p21 and downregulation of the anti-apoptotic protein XIAP in both LSCs and AN-LSCs. A further increase in the pro-apoptotic Caspase-10, together with a decrease in the pro-apoptotic Bax, was detected only in LSCs and not in AN-LSCs. In contrast, a reduction in the anti-apoptotic protein Survivin was found exclusively in AN-LSCs and was not present in LSCs. These findings indicate that while LSCs can temporarily withstand metabolic stress, sustained hyperglycemia ultimately overwhelms their protective capacity and activates apoptotic pathways. Notably, AN-LSCs exhibit a greater susceptibility to late-phase apoptotic collapse. Understanding the molecular mechanisms governing this transition offers therapeutic opportunities by attenuating the pro-apoptotic signaling—to preserve LSCs viability and maintain corneal integrity in metabolic and degenerative ocular diseases such as diabetic keratopathy and aniridia-associated keratopathy.

CRediT authorship contribution statement

Shanhe Liu: Writing – review & editing, Writing – original draft, Visualization, Validation, Supervision, Software, Resources, Project administration, Methodology, Investigation, Formal analysis, Data curation, Conceptualization. **Shuailin Li:** Writing – review & editing. **Shao-Lun Hsu:** Writing – review & editing. **Fabian N. Fries:** Writing – review & editing. **Zhen Li:** Writing – review & editing. **Swarnali Kundu:** Writing – review & editing. **Virendra Kumar:** Writing – review & editing. **Berthold Seitz:** Writing – review & editing. **Maryam Amini:** Writing – review & editing. **Shweta Suiwal:** Writing – review & editing. **Nóra Szentmáry:** Writing – review & editing, Supervision, Methodology, Investigation, Data curation, Conceptualization. **Tanja Stachon:** Writing – review & editing, Methodology, Data curation, Conceptualization.

Declaration of competing interest

The authors declare that they have no known competing financial interests or personal relationships that could have appeared to influence the work reported in this paper.

Acknowledgements

The work of Shanhe Liu, Shuailin, Li, Shao-Lun Hsu, Fabian N. Fries, Zhen Li, Swarnali Kundu, Maryam Amini, Shweta Suiwal, Tanja Stachon and Nóra Szentmáry at the Dr. Rolf M. Schwiete Center has been supported by the Dr. Rolf M. Schwiete Foundation (08/2017). The work of Shanhe Liu (202309210134), Shuailin Li (202508080040) and Zhen Li (202208080086) has been supported by the China Scholarship Council. The author(s) received no specific funding for this work.

Data availability

Data will be made available on request.

References

Allen, D.A., Yaqoob, M.M., Harwood, S.M., 2005. Mechanisms of high glucose-induced apoptosis and its relationship to diabetic complications. J. Nutr. Biochem. 16, 705–713.
Bettahi, I., Sun, H., Gao, N., Wang, F., Mi, X., Chen, W., Liu, Z., Yu, F.S., 2014. Genome-wide transcriptional analysis of differentially expressed genes in diabetic, healing corneal epithelial cells: hyperglycemia-suppressed TGFbeta3 expression contributes to the delay of epithelial wound healing in diabetic corneas. Diabetes 63, 715–727.
Borroni, D., Wowra, B., Romano, V., Boyadzhieva, M., Ponzin, D., Ferrari, S., Ahmad, S., Parekh, M., 2018. Simple limbal epithelial transplantation: a review on current approach and future directions. Surv. Ophthalmol. 63, 869–874.
Brandt, S., Kopp, A., Grage, B., Knabbe, C., 2003. Effects of tamoxifen on transcriptional level of transforming growth factor beta (TGF-beta) isoforms 1 and 2 in tumor tissue during primary treatment of patients with breast cancer. Anticancer Res. 23, 223–229.
Buonfiglio, F., Wasielica-Poslednik, J., Pfeiffer, N., Gericke, A., 2024. Diabetic keratopathy: redox signaling pathways and therapeutic prospects. Antioxidants 13.
Cepas, V., Collino, M., Mayo, J.C., Sainz, R.M., 2020. Redox signaling and advanced glycation endproducts (AGEs) in diet-related diseases. Antioxidants 9.
Chen, Y.H., Chen, Z.W., Li, H.M., Yan, X.F., Feng, B., 2018. AGE/RAGE-Induced EMP release via the NOX-derived ROS pathway. J. Diabetes Res. 2018, 6823058.
Currier, A.W., Kolb, E.A., Gorlick, R.G., Roth, M.E., Gopalakrishnan, V., Sampson, V.B., 2019. p27/Kip1 functions as a tumor suppressor and oncoprotein in osteosarcoma. Sci. Rep. 9, 6161.
Daruich, A., Duncan, M., Robert, M.P., Lagali, N., Semina, E.V., Aberdam, D., Ferrari, S., Romano, V., des Roziers, C.B., Benkortebi, R., De Vergnes, N., Polak, M., Chiambaretta, F., Nischal, K.K., Behar-Cohen, F., Valleix, S., Bremond-Gignac, D., 2023. Congenital aniridia beyond Black eyes: from phenotype and novel genetic mechanisms to innovative therapeutic approaches. Prog. Retin. Eye Res. 95, 101133.
Dobi, A., Bravo, S.B., Veeren, B., Paradela-Dobarro, B., Alvarez, E., Meilhac, O., Viranaicken, W., Baret, P., Devin, A., Rondeau, P., 2019. Advanced glycation end-products disrupt human endothelial cells redox homeostasis: new insights into reactive oxygen species production. Free Radic. Res. 53, 150–169.
Foster, C.S., Tufail, F., Waheed, N.K., Chu, D., Miserocchi, E., Baltatzis, S., Vredeveld, C. M., 2003. Efficacy of etanercept in preventing relapse of uveitis controlled by methotrexate. Arch. Ophthalmol. 121, 437–440.
Funderburgh, J.L., Funderburgh, M.L., Du, Y., 2016. Stem cells in the limbal stroma. Ocul. Surf. 14, 113–120.
Hingorani, M., Hanson, I., van Heyningen, V., 2012. Aniridia. Eur. J. Hum. Genet. 20, 1011–1017.
Kim, J., Kim, C.S., Sohn, E., Jeong, I.H., Kim, H., Kim, J.S., 2011. Involvement of advanced glycation end products, oxidative stress and nuclear factor-kappaB in the development of diabetic keratopathy. Graefes Arch. Clin. Exp. Ophthalmol. 249, 529–536.
Kim, S.J., Li, J., 2013. Caspase blockade induces RIP3-mediated programmed necrosis in toll-like receptor-activated microglia. Cell Death Dis. 4, e716.
Lagali, N., Eden, U., Utheim, T.P., Chen, X., Riise, R., Dellby, A., Fagerholm, P., 2013. In vivo morphology of the limbal palisades of vogt correlates with progressive stem cell deficiency in aniridia-related keratopathy. Investig. Ophthalmol. Vis. Sci. 54, 5333–5342.
Landsend, E.C.S., Lagali, N., Utheim, T.P., 2021. Congenital aniridia - a comprehensive review of clinical features and therapeutic approaches. Surv. Ophthalmol. 66, 1031–1050.
Latta, L., Figueiredo, F.C., Ashery-Padan, R., Collinson, J.M., Daniels, J., Ferrari, S., Szentmary, N., Sola, S., Shalom-Feuerstein, R., Lako, M., Xapelli, S., Aberdam, D., Lagali, N., 2021a. Pathophysiology of aniridia-associated keratopathy: developmental aspects and unanswered questions. Ocul. Surf. 22, 245–266.
Latta, L., Knebel, I., Bleil, C., Stachon, T., Katiyar, P., Zussy, C., Fries, F.N., Kasmann-Kellner, B., Seitz, B., Szentmary, N., 2021b. Similarities in DSG1 and KRT3 downregulation through retinoic acid treatment and PAX6 knockdown related expression profiles: does PAX6 affect RA signaling in limbal epithelial cells? Biomolecules 11.
Latta, L., Ludwig, N., Krammes, L., Stachon, T., Fries, F.N., Mukwaya, A., Szentmary, N., Seitz, B., Wowra, B., Kahraman, M., Keller, A., Meese, E., Lagali, N., Kasmann-Kellner, B., 2021c. Abnormal neovascular and proliferative conjunctival phenotype in limbal stem cell deficiency is associated with altered microRNA and gene expression modulated by PAX6 mutational status in congenital aniridia. Ocul. Surf. 19, 115–127.
Li, S., Stachon, T., Liu, S., Li, Z., Hsu, S.L., Kundu, S., Fries, F.N., Seitz, B., Amini, M., Suiwal, S., Szentmary, N., 2025a. Increased sensitivity of primary aniridia limbal stromal cells to travoprost, leading to elevated migration and MMP-9 protein levels, in vitro. PLoS One 20, e0326967.
Li, Z., Stachon, T., Hacker, S., Fries, F.N., Chai, N., Seitz, B., Shi, L., Hsu, S.L., Li, S., Liu, S., Amini, M., Suiwal, S., Szentmary, N., 2025b. Increased glucose concentration modifies TGF-beta1 and NFkappaB signaling pathways in aniridia limbal fibroblasts, in vitro. Exp. Eye Res. 250, 110163.
Li, Z., Stachon, T., Zimmermann, J., Trusen, S., Fries, F.N., Berger, M., Suiwal, S., Chai, N., Seitz, B., Shi, L., Amini, M., Szentmary, N., 2025c. Expression of PAX6 and keratocyte-characteristic markers in human limbal stromal cells of congenital aniridia and healthy subjects, in vitro. Curr. Eye Res. 50, 362–372.
Li, Z., Szentmary, N., Fries, F.N., Suiwal, S., Chai, N., Seitz, B., Shi, L., Amini, M., Stachon, T., 2024. Effect of ritanserin and duloxetine on the gene expression of primary aniridia and healthy human limbal stromal cells, in vitro. Ophthalmol Ther 13, 2931–2950.

Liu, S., Li, S., Hsu, S.L., Fries, F.N., Li, Z., Kundu, S., Seitz, B., Amini, M., Suiwal, S., Zimmermann, J., Trusen, S., Stachon, T., Szentmary, N., 2025a. Altered Bcl-2/Caspase signaling and hypoxia-induced apoptosis in primary human aniridia limbal stromal cells, in CoCl2 mediated hypoxic stress, in vitro. PLoS One 20, e0328157.

Liu, S., Li, S., Hsu, S.L., Fries, F.N., Li, Z., Kundu, S., Seitz, B., Amini, M., Suiwal, S., Stachon, T., Szentmary, N., 2025b. Elevated anti-apoptotic shift in primary human aniridia limbal stromal cells following 48 hours supraphysiologic submitted exposure, in vitro. PLoS One 2025 submitted for publication.

Pellinen, P., Huhtala, A., Tolonen, A., Lokkila, J., Maenpaa, J., Uusitalo, H., 2012. The cytotoxic effects of preserved and preservative-free prostaglandin analogs on human corneal and conjunctival epithelium in vitro and the distribution of benzalkonium chloride homologs in ocular surface tissues in vivo. Curr. Eye Res. 37, 145–154.

Ramaesh, K., Ramaesh, T., Dutton, G.N., Dhillon, B., 2005. Evolving concepts on the pathogenic mechanisms of aniridia related keratopathy. Int. J. Biochem. Cell Biol. 37, 547–557.

Rocha de Lossada, C., Pagano, L., Gadhvi, K.A., Borroni, D., Figueiredo, G., Kaye, S., Romano, V., 2020. Persistent loss of marginal corneal arcades after chemical injury. Indian J. Ophthalmol. 68, 2543–2544.

Samant, M., Chauhan, B.K., Lathrop, K.L., Nischal, K.K., 2016. Congenital aniridia: etiology, manifestations and management. Expert Rev Ophthalmol 11, 135–144.

Santos, J.M., Kowluru, R.A., 2011. Role of mitochondria biogenesis in the metabolic memory associated with the continued progression of diabetic retinopathy and its regulation by lipoic acid. Investig. Ophthalmol. Vis. Sci. 52, 8791–8798.

Shamloo, B., Usluer, S., 2019. p21 in cancer research. Cancers (Basel) 11.

Shi, L., Yu, X., Yang, H., Wu, X., 2013. Advanced glycation end products induce human corneal epithelial cells apoptosis through generation of reactive oxygen species and activation of JNK and p38 MAPK pathways. PLoS One 8, e66781.

Souers, A.J., Leverson, J.D., Boghaert, E.R., Ackler, S.L., Catron, N.D., Chen, J., Dayton, B.D., Ding, H., Enschede, S.H., Fairbrother, W.J., Huang, D.C., Hymowitz, S. G., Jin, S., Khaw, S.L., Kovar, P.J., Lam, L.T., Lee, J., Maecker, H.L., Marsh, K.C., Mason, K.D., Mitten, M.J., Nimmer, P.M., Oleksijew, A., Park, C.H., Park, C.M., Phillips, D.C., Roberts, A.W., Sampath, D., Seymour, J.F., Smith, M.L., Sullivan, G. M., Tahir, S.K., Tse, C., Wendt, M.D., Xiao, Y., Xue, J.C., Zhang, H., Humerickhouse, R.A., Rosenberg, S.H., Elmore, S.W., 2013. ABT-199, a potent and selective BCL-2 inhibitor, achieves antitumor activity while sparing platelets. Nat Med 19, 202–208.

Taguchi, K., Fukami, K., 2023. RAGE signaling regulates the progression of diabetic complications. Front. Pharmacol. 14, 1128872.

Tien, T., Zhang, J., Muto, T., Kim, D., Sarthy, V.P., Roy, S., 2017. High glucose induces mitochondrial dysfunction in retinal muller cells: implications for diabetic retinopathy. Investig. Ophthalmol. Vis. Sci. 58, 2915–2921.

van Velthoven, A.J.H., Utheim, T.P., Notara, M., Bremond-Gignac, D., Figueiredo, F.C., Skottman, H., Aberdam, D., Daniels, J.T., Ferrari, G., Grupcheva, C., Koppen, C., Parekh, M., Ritter, T., Romano, V., Ferrari, S., Cursiefen, C., Lagali, N., LaPointe, V.L. S., Dickman, M.M., 2023. Future directions in managing aniridia-associated keratopathy. Surv. Ophthalmol. 68, 940–956.

Xu, K., Yu, F.S., 2011. Impaired epithelial wound healing and EGFR signaling pathways in the corneas of diabetic rats. Investig. Ophthalmol. Vis. Sci. 52, 3301–3308.

Zhang, L.Y., Lin, R.T., Chen, H.R., Yang, Y.C., Lin, M.F., Tian, L.G., Pan, Z.Q., Lin, L., Zhu, L.L., Gu, Z.J., Chen, X.W., Li, Y.J., Chen, S., Cai, S.Y., 2021. High glucose activated cardiac fibroblasts by a disruption of mitochondria-associated membranes. Front. Physiol. 12, 724470.